AGU100 ADVANCING EARTH AND SPACE SCIENCE

Geophysical Research Letters

RESEARCH LETTER
10.1029/2018GL080516

Key Points:
- Thirty-five years of satellite data reveal an MCS intensification trend over equatorial Africa in February
- There is a strong interannual correlation between Congo MCS intensity and temperature over the Eastern Sahel and Sahara
- Upper-level wave trains from the extratropics are implicated in Sahelian warm events

Correspondence to:
C. M. Taylor,
cmt@ceh.ac.uk

Citation:
Taylor, C. M., Fink, A. H., Klein, C., Parker, D. J., Guichard, F., Harris, P. P., & Knapp, K. R. (2018). Earlier seasonal onset of intense mesoscale convective systems in the Congo Basin since 1999. *Geophysical Research Letters, 45*, 13,458–13,467. https://doi.org/10.1029/2018GL080516

Received 17 SEP 2018
Accepted 1 DEC 2018
Accepted article online 7 DEC 2018
Published online 19 DEC 2018

Earlier Seasonal Onset of Intense Mesoscale Convective Systems in the Congo Basin Since 1999

Christopher M. Taylor[1,2], Andreas H. Fink[3], Cornelia Klein[1], Douglas J. Parker[4], Françoise Guichard[5], Philip P. Harris[1,2], and Kenneth R. Knapp[6]

[1]Centre for Ecology and Hydrology, Wallingford, UK, [2]National Centre for Earth Observation, Wallingford, UK, [3]Institute for Meteorology and Climate Research, Karlsruhe Institute for Technology, Karlsruhe, Germany, [4]School of Earth and Environment, University of Leeds, Leeds, UK, [5]Centre National de Recherches Météorologique (CNRM), UMR 3589, Centre de la Recherche Scientifique (CNRS) and Méteo-France, Toulouse Cedex, France, [6]NOAA/National Centers for Environmental Information, Asheville, NC, USA

Abstract Mesoscale convective systems (MCSs) produce some of the most intense rainfall on the planet, and their response to climate variability and change is rather uncertain. Under global warming, increased water vapor is expected to intensify the most extreme rain events and enhance flood frequency. However, MCS dynamics are also sensitive to other atmospheric variables, most notably, wind shear. Here we build on a recent study showing strong MCS intensification in the African Sahel, and examine evidence of similar trends elsewhere in tropical Africa. Using satellite data, we find a remarkable increase post-1999 in intense MCS frequency over the Congo Basin during the month of February. This earlier onset of the spring rainy season has been accompanied by strong increases in the February meridional temperature gradient and associated wind shear. This supports the hypothesis that contrasts in warming across the continent can drive important decadal-scale trends in storm intensity.

Plain Language Summary Understanding how storms will change in a warming world is a major scientific challenge and one that has important impacts on society. Changes in the amount of atmospheric water vapor is considered to be the major driver for historical and future trends in intense storms. Here we examine how the intensity of storms over equatorial Africa has evolved since the early 1980s. Building on a previous landmark study over the semiarid Sahel region of North Africa, we identify that substantial storm intensification has taken place over the tropical forests of the Congo Basin, in February, marking the start of the first rainy season. The number of intense storms in that month has jumped by more than 100% since 1999, coinciding with a warming of 2 °C in the more arid parts of North-Eastern Africa. Episodes of high temperatures over Sudan change the winds and moisture over the Congo Basin, and these factors favor more explosive storms. This provides additional evidence that African storms are sensitive to changes in temperature gradients across the continent and not just atmospheric humidity. These gradients are expected to increase with climate change, likely raising the frequency of flood events.

1. Introduction

Understanding the relationships between intense rain events and the larger-scale climate is a major challenge for scientists. Under global warming, the most intense events are expected to strengthen due to increased humidity. Intensification of rainfall extremes potentially enhances flood frequency and increases soil erosion, important factors for decision makers in infrastructure and agriculture. A large body of research has examined observational trends in extreme rainfall (Min et al., 2011; Westra et al., 2013), scaling relationships with temperature (Kai et al., 2017; Lenderink & van Meijgaard, 2008), and future projections in intense rain (O'Gorman, 2015; Westra et al., 2014).

A complication for our physical understanding of this problem comes from mesoscale convective systems (MCSs; Houze, 2004), characterized by organized mesoscale dynamics. In particular, the extent to which MCS rainfall intensity is controlled by atmospheric moisture remains an open question (Muller, 2013; Prein et al., 2017; Singleton & Toumi, 2013), not least because wind shear also affects organized convection (Alfaro, 2017; Rotunno et al., 1988; Thorpe et al., 1982). Highly organized MCSs are the major rain-bearing rainfall systems across much of tropical Africa (Jackson et al., 2009; Nesbitt et al., 2006). In the Sahel, MCSs produce approximately 90% of total precipitation (Mathon et al., 2002), falling to 56% at

the Guinea Coast (Maranan et al., 2018). Taylor et al. (2017; henceforth T17) identified a tripling in the frequency of intense Sahelian MCSs observed over the last 35 years, a trend with important hydrological consequences. They estimated a decrease in the mean cloud-top temperature of Sahelian MCSs of 0.78 °C per decade, consistent with deeper, more energetic convective updraughts, and more intense rainfall. Rather than humidity, T17 proposed that the trend in meridional temperature gradient (driven primarily by increasing greenhouse gas concentration) was the key driver. As in other arid low-latitude regions, the Sahara has been warming more rapidly than moister tropical regions (Cook & Vizy, 2015; Zhou, 2016), and this trend is projected to continue. For the Sahel, which lies between the Sahara and the moist tropical forests of the Congo Basin and Guinea Coast, this implies increasing baroclinicity. T17 argued that this can affect MCS intensity via increased wind shear, midtropospheric temperature, relative humidity, and synoptic activity.

According to T17, trends in African MCS intensity are most pronounced during the Sahelian wet season (June–September), although significant signals in sub-Sahelian West Africa during other seasons were found. They found no evidence of widespread trends at the seasonal or annual time scales in the Congo Basin, a region known for very intense convection and lightning associated with westward propagating MCSs (Albrecht et al., 2016; Zipser et al., 2006). However, Raghavendra et al. (2018) subsequently identified a trend toward more intense thunderstorms in the Congo Basin during the April–June season (AMJ). In this paper, we use a similar approach to T17 to examine sub-Sahelian MCS trends and their relationship with meridional temperature gradients; such analysis can shed light on the role of forced versus natural climate variability in changing hydrological extremes. In the next section, we describe the data sets, then assess the relationships between monthly trends in temperature and MCS intensity. Motivated by the strong trends found in these variables during February, the remainder of the paper focuses on this month, which marks the onset of the intense MCS season in the northern Congo Basin.

2. Data

The primary data used are cloud-top temperatures from thermal infrared measurements onboard the Meteosat series of geostationary satellites for the period 1982 to 2016. The Meteosat programme was designed for operational weather forecasting rather than the climate community, and the original data set contains discontinuities and biases associated with changes in satellite and instrument drifts (Maidment et al., 2014). To minimize the influence of these artifacts, we use the reprocessed GridSat Climate Data Record version (Knapp et al., 2011) available every 3 hr at a resolution of 0.07°. Data are available from 1982 onward, though in the early years there are periods of no observations. The data set benefits from an absolute calibration using radiometer measurements from polar-orbiting satellites, and a second cross-calibration with an infrared radiation sounder (Knapp, 2008). The estimated calibration uncertainty in the temperature is less than 0.1 °C per decade.

Following T17, we define MCSs as contiguous areas of cold cloud exceeding 25,000 km^2 for a given temperature threshold. At the event time scale, MCSs at colder thresholds (higher altitudes) are associated with an increased probability of intense rainfall (T17, Klein et al., 2018). Here we focus on thresholds of −40 and −70 °C and term these systems respectively MCSs, and intense MCSs. We sample these systems every 3 hr between 1500 and 0300 UTC, a period that includes most intense MCS activity. For presentation, most of the analysis is based on images at 1800 UTC. This corresponds to a local time of between 2000 (30°E) and 1720 (10°W) and follows the maximum vertical extension phase (Futyan & Genio, 2007; Proud, 2015). Similar results are obtained using an alternative areal threshold of 5,000 km^2, and using images at 2100 and 0000 UTC (mature phase), though the frequency of MCSs decreases as the night progresses. Coverage of MCSs (%) is computed at the 1° scale, based on the fractional area containing pixels within contiguous cold cloud structures, while MCS frequency (per day) is computed from the average number of discrete MCSs centered within a specified larger region over a month. Months are excluded where five or fewer days of data are available; sampling at 1800 UTC, this amounts to only 4 out of 420 months. Previous work (T17) has shown that this measure of MCS frequency is robust to changes in measurement technology, notably the transition from Meteosat First to Second Generation, which occurs in July 2006 in the GridSat data set. Finally, the MCS temperature is defined as the mean temperature of pixels within a system defined with a −40 °C threshold and is considered a measure of convective intensity.

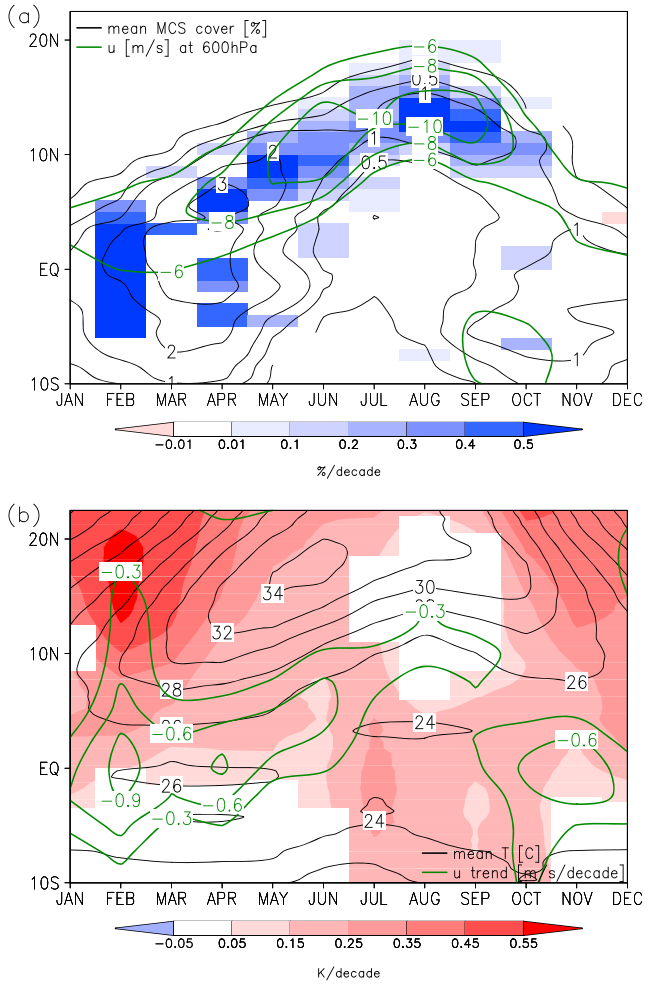

Figure 1. Trends (shading; decade^{-1}) and mean values (black contours) by month and latitude in (a) intense (−70 °C) MCS coverage (%) at 1800 UTC, and (b) 2 m temperature from CRU (°C), across West and central Africa (15°W to 28°E) for the period 1982–2016. Trends are only shown where significant at the 95% level (two-tailed *t* test). Solid green contours show the mean (a; m/s) and trend (b; ms^{-1} decade^{-1}) of zonal wind at 600 hPa, indicative of the African easterly jet. All data sets are averaged over land points only. MCS = mesoscale convective system.

We characterize long-term trends in temperature using several observational data sets. The CRU TS4.01 data set (Harris et al., 2014) provides a gridded compilation (0.5° resolution) of monthly mean 2 m temperatures, available until 2016. The contributing network of stations is heterogeneous across Africa, with notably few stations within the Congo Basin and the Sahara Desert. More spatially consistent information on temperature trends can be obtained from spaceborne microwave sounding instruments, and we use the MSU compilation (Christy et al., 2000) version 5.6. This provides a temperature estimate of the lowest 8 km of the column but weighted heavily toward the bottom 3–4 km. We also use monthly compilations of global land (CRUTEM4; Jones et al., 2012) and ocean (HadISST; Rayner et al., 2003) temperature gridded at 5° and 1° respectively. To complement these data we use the ERA-Interim (Dee et al., 2011) atmospheric reanalysis product. The network of available rain gauges in central Africa is sparse and compromises the quality of gauge-based trends of monthly rainfall in products such as CRU TS4.01. Instead, we use the TRMM3B43 rainfall product, based on merging data from multiple satellites (including Meteosat) with gauges where available, covering the period from 1998 to the present (Huffman et al., 2007).

3. Results

3.1. Annual Cycle

The seasonal migration of intense MCS activity is depicted in Figure 1a, sampled at 1800 UTC, zonally averaged over land points between 15°W and 28°E. A band of intense MCS occurrence advances northward from February to August, in phase with the rain belt. During the southward retreat, particularly during October to January, cloud-top temperatures within the band are notably higher, as evident from lower intense MCS coverage. This seasonal asymmetry in intensity coincides with an asymmetric evolution of the AEJ in the Northern Hemisphere (stronger easterlies during the northward advance), suggestive of a shear control on the seasonal evolution of MCS intensity. The link to shear is consistent with analysis over southern West Africa (Maranan et al., 2018) and the Congo Basin (Laing et al., 2011). Significant positive trends in MCS cover are evident over much of the band north of 5°N, particularly during the Sahelian wet season (12–18°N, June to September). By contrast, only during the months of February and April are widespread significant trends evident over the Congo Basin (defined as 5°S to 5°N). In February, the Congo signal amounts to a 114% increase over 35 years compared to the mean for that period. By the same measure, there is a 127% increase for the Sahelian wet season (June–September), and a 41% increase in April over the Congo. This monthly analysis indicates that the trend for AMJ identified by Raghavendra et al. (2018) is dominated by an increase in April, which in turn is weaker (markedly so in relative terms) than the positive trend in February.

Trends in zonal mean surface air temperatures (Figure 1b) are generally positive ($P < 0.05$) across Northern Africa, and are particularly strong to the north of the MCS belt. The strongest warming trend occurs ahead of the hottest months of the year, with more modest warming in the months following the rainy season. Strong warming also occurs in the Sahara (20–30°N; Evan et al., 2014), particularly July–September (Vizy & Cook, 2017), though observations used in this particular gridded data set are too sparse to provide reliable regional trends there. The strong warming trend in more arid regions and seasons is consistent with anthropogenic forcing (Zhou, 2016). By contrast, wet season temperature trends are weak south of the Equator and also in the Sahel at the peak of the monsoon. After the wet season, transpiration persists for several months, buffering any potential anthropogenic warming of the planetary boundary layer (PBL).

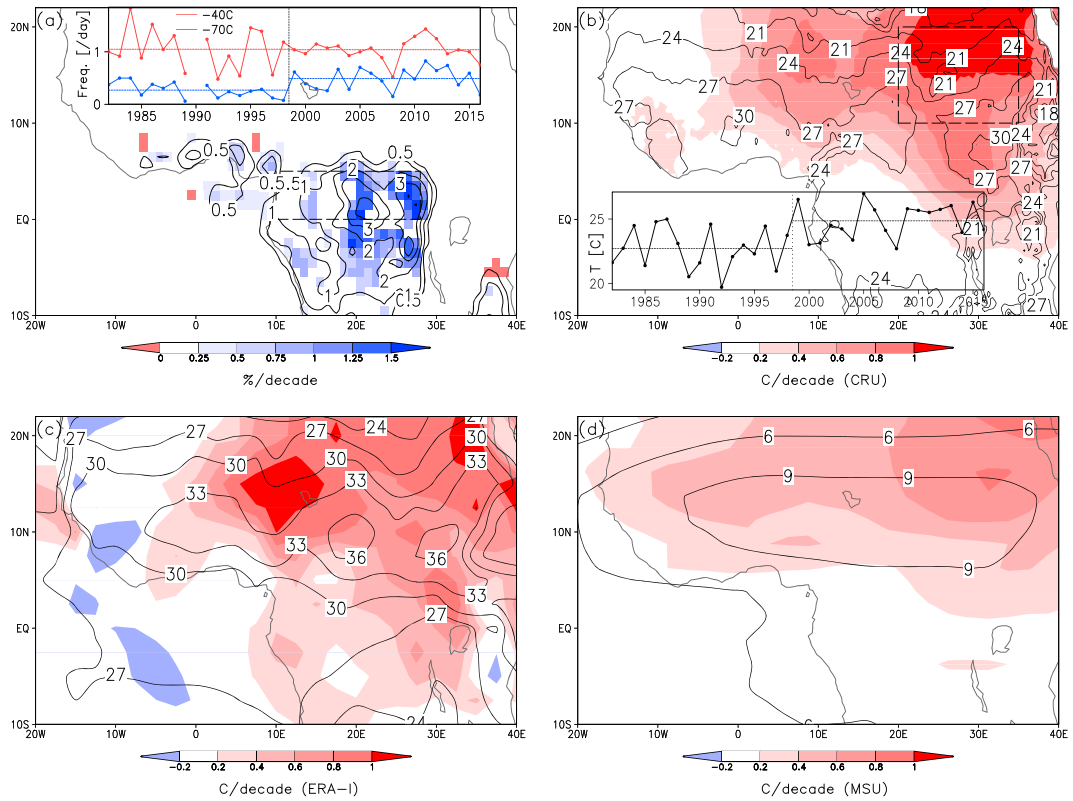

Figure 2. February trends in (a) frequency of intense mesoscale convective systems (sampled at 1800 UTC; % decade^{-1}) and temperature (°C decade^{-1}) from (b) CRU, (c) ERA-Interim, and (d) MSU. Temperature trends all use monthly mean data, at 2 m (b and c) and over the lower troposphere (d). Insets depict time series of February mean (a) mesoscale convective system frequency (day^{-1}) observed at 1800 UTC over the northern Congo (dashed rectangle; 10–28°E, 0–5°N) for thresholds of −40 °C and −70 °C, and (b) temperature from CRU over the East Sahel (dashed rectangle; 20–35°E, 10–20°N). Horizontal lines depict the mean values of these variables for the periods 1982–1998 and 1999–2016.

Given relatively weak warming in the moist tropics throughout the year, the above changes produce stronger meridional temperature gradients. The month of February stands out, with Sahelian warming driving an increase in land temperature contrast of 0.62 °C between the equator and 15°N over 35 years. This coincides with the strongest increase in the AEJ (more than 3 m/s over 35 years), and as noted above, strong MCS intensification in the Congo. Taken together, these data support the hypothesis that warming in North Africa's semiarid and arid regions (relative to the moist tropics) can increase convective intensity within the migrating rain belt, via increases in wind shear. Compared with other months, February provides particularly strong trends in baroclinicity, and we therefore focus the remainder of the study on that month, which corresponds to the onset of the MCS season in the moist tropics of Northern Africa.

3.2. Trends and Correlations in February MCSs

The February trends in intense MCS coverage and temperature across Africa are shown in Figure 2. The largest trends (in absolute terms) in MCSs at 1800 UTC occur in the eastern Congo Basin, in areas where MCSs preferentially initiate during the afternoon. The maximum in the trend appears progressively further west when sampling later in the evening and overnight (not shown), moving westward with the systems themselves (Laing et al., 2011). Temperature data from three different sources (gridded in situ observations, reanalysis, and lower tropospheric soundings from satellites) all indicate that the strong warming in Sahelian latitudes is more pronounced in the east, though the details amongst the data sets differ. Averaged over the lower troposphere (Figure 2d), the temperature trend is weaker than at the surface, consistent with maximum warming within the PBL. Maximum warming rates occur to the north of the February climatological heat low (located at 5–10°N; Lavaysse et al., 2009). The similarity of the three warming patterns lends confidence to the existence of a particularly strong trend in the meridional temperature gradient during February.

The trend in intense MCSs is far from linear over the 35-year period (Figure 2a, inset). For the first half of the record (to 1998), there is on average one intense MCS every 3.7 days in the northern Congo Basin at 1800 UTC. From 1999 to 2016, that frequency nearly doubles, to one event every 2 days, an increase significant at the 99.9% level. By contrast, the average frequency of all MCSs (defined at a temperature threshold of −40 °C) shows no increase between the two periods. There is no similar jump in intense MCSs in other months from 1998 to 1999, and it therefore seems unlikely to be an artifact of the Meteosat measurements. Moreover, the increase in intense storm frequency coincides with a shift to higher February temperatures in the Eastern Sahel (Figure 2b, inset; difference of 2.2 °C between the two periods). The relationship between intense MCS frequency and monthly rainfall can be assessed using TRMM3B43 data from 1998 onward. Averaged over the Northern Congo region, February rainfall is well correlated ($r = 0.66$, $p < 0.005$) with intense MCS frequency sampled at 1800 UTC, becoming more so ($r = 0.74$, $p < 0.001$) when extending the sampling window from 1500 to 0300 UTC. This implies that the shift to more intense February MCSs from 1999 onward is likely associated with an earlier onset of the rainy season in the N. Congo. The length of wet and dry seasons is an important constraint on plant productivity for tropical forest, and the improvement in growing conditions in February may have partially offset the deleterious effects of the more recent drying trend during AMJ (Zhou et al., 2014). Unlike in February, we find no significant correlation between monthly rainfall and intense MCS frequency during AMJ, consistent with the results of Raghavendra et al. (2018).

We now consider temporal correlations between February-mean MCS temperature (a proxy for MCS intensity) and key atmospheric variables in ERA-Interim. On average, MCS temperatures are 2.15 °C colder in the second half of the period (Figure 3c, inset). As expected from the discussion above, there is a strong positive correlation between PBL temperature (850 hPa) in the Eastern Sahel, and Congo MCS intensity (Figure 3a). A significant negative correlation between those variables also exists across northwestern Africa. Overlying the warmer PBL in the E. Sahel, anticyclonic flow at 600 hPa strengthens. This circulation enhances the AEJ (between 2 and 6°N) during years with intense Congo MCSs. At 925 hPa (Figure 3b), the extension of the heat low into the Sahel drives anomalous southwesterly flow between 5 and 10°N. The moisture convergence associated with this anomaly accounts for the increased low-level moisture over the Central African Republic and northern Cameroon. The spatial structure of the Sahelian PBL temperature anomaly closely resembles a pattern of increased downward (and upward) long-wave fluxes at the surface (Figure 3c). South of 10°N, the long-wave signal is associated with increased cloud cover (not shown), but to the north, the PBL is very dry (mean of less than 4 g/kg; Figure 3c), and there is almost no cloud cover.

The intensification of MCSs is correlated with a large scale anomaly pattern in upper-level geopotential height (Figure 3d). Stronger MCSs are associated with positive 300-hPa heights over North-Western Russia, North-Eastern Africa/Arabia, and Southern China, and negative values over central Europe. This pattern resembles the negative phase of the Eastern Atlantic/Western Russia pattern (Figure 3c in Ionita, 2014), which has exhibited a negative trend over the last 20 years in February. More intense Congo MCSs are also correlated to SSTs in the North Atlantic and Arctic Oceans (Figure 3d), notably the strong warming in the western tropical and subtropical Atlantic, south of Newfoundland and in the European Arctic (e.g., Huang et al., 2018). Potential links between MCS intensification and these decadal-scale features of the global climate merit further study. In summary, more intense Congo MCSs are correlated with an upper-level anticyclone over North-Eastern Africa, a northward excursion of the heat low into the Eastern Sahel, and associated enhanced midlevel easterlies on its southern flank.

3.3. Event-Based Analysis

Using ERA-Interim, we now compare days when intense and weak Congo MCSs are observed. For every February day at 1800 UTC, we compute the mean temperature of MCSs in the North-Eastern Congo (0–5°N, 20–28°E). We choose this region as it exhibits high values in both the mean and trend of intense MCSs. To minimize the impact of longer-term trends, only events from 2007 to 2016 are used. Days with MCS coverage less than 10% are excluded (51 out of 283 days). We then create two subsets, based on days with the most intense (coldest quartile, mean = −58.1 °C) and least intense (warmest quartile, mean = −50.5 °C) events. Figures 4a and 4b illustrate the mean humidity and zonal wind profiles averaged across the North-Eastern Congo for the two composites. Days with intense MCSs are on average 1.9 g/kg moister below 850 hPa than their weak counterparts and exhibit a stronger (2.6 m/s) AEJ. Both of these factors likely favor more intense MCS.

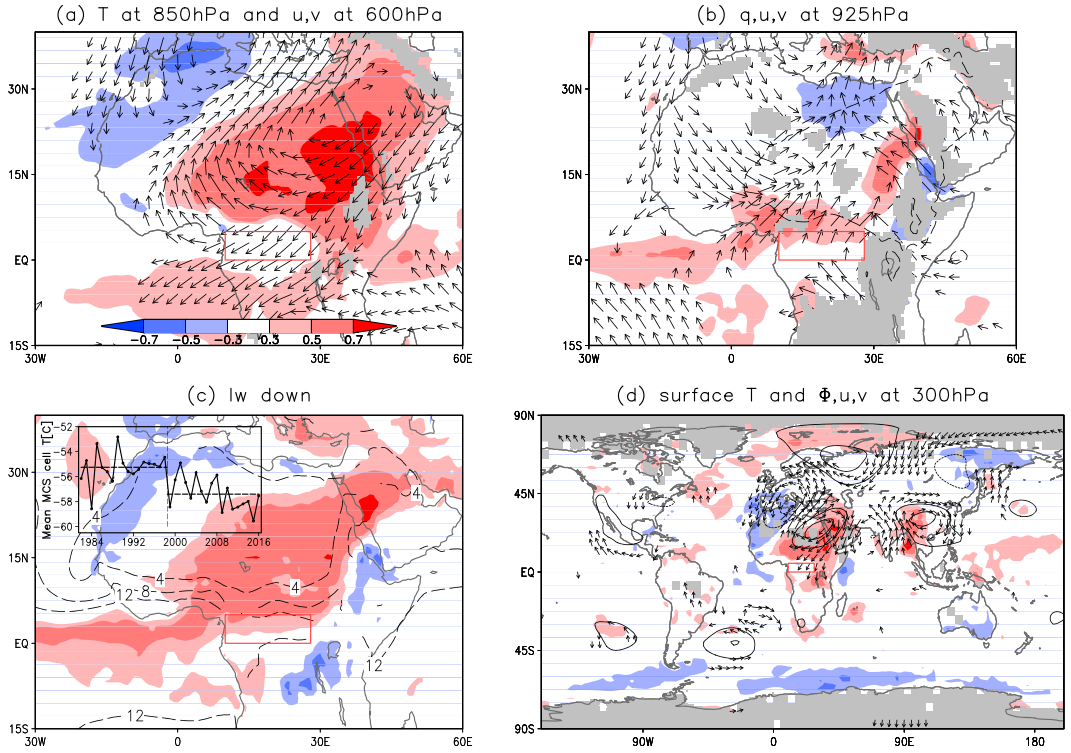

Figure 3. Correlation coefficients between mean mesoscale convective system (MCS) intensity in the N. Congo (red box) and selected variables from ERA-I for the month of February for the years 1982–2016. The (a) 850-hPa temperature (shading) and 600-hPa winds (vectors); (b) 925-hPa specific humidity (shading) and 925-hPa winds (vectors); (c) downwelling long-wave radiation at the surface (shading); and (d) surface temperature (shading), 300 hPa geopotential height (contours), and winds (vectors). Intensity is measured by the negative value of MCS temperature, so that positive (red) values indicate conditions associated with more intense MCS. Areas masked in gray indicate missing data or pressure levels below the surface. Temperature data in (d) comes from HadISST (ocean) and CRUTEM4 (land). Wind vectors are only plotted where regressions are significant at the 95% level for at least one component. Black dashed contours indicate in (b) correlation coefficient of 0.5 with 850-hPa temperature (i.e., repeated from (a)), and in (c) the mean 925-hPa specific humidity (g/kg; only plotted above the surface). The time series of MCS mean temperature is depicted in the inset of (c), with mean values for the years up to and after 1998 shown as horizontal lines.

Differences in evolving synoptic features between the two subsets are shown in Figures 4c–4h. At 5 and 3 days ahead of an intense event (Figures 4e and 4f), enhanced 300-hPa heights are evident over North-Eastern Africa and the Middle East, as part of a wave train from the extratropical Atlantic Ocean (e.g., Figure 4g). Over North-Eastern Africa, this triggers strong warming and enhanced southerly wind anomalies at 850 hPa. By day −3, low-level composite temperature differences exceed 4.5 °C in parts of the Eastern Sahel and Sahara (Figure 4f). In subsequent days, the low-level warm feature propagates equatorward into the Eastern Sahel, and away from the weakening upper level ridge (Figures 4c and 4g). This propagation may be linked to enhanced advection of warmer air from the climatological heat low (5–10°N). The timing and location of warming also suggests a role for moisture convergence and resulting changes in long-wave radiative processes, with increases in PBL moisture and surface (downward and upward) long-wave fluxes of the order of 0.5 g/kg and 15 W/m^2 respectively averaged across the E. Sahel (not shown). Irrespective of the detail of its propagation mechanism, when the warm anomaly reaches 12°N (days −1 to 0; Figure 4c), its presence has an important impact on the environment in which Congo MCSs develop. A warmed E. Sahel drives enhanced moisture convergence into central Africa north of the Equator and increases shear through stronger midlevel easterlies. The effect of these changes are evident in Figures 4a and 4b, respectively.

The location of the heat low anomaly in the days preceding intense Congo MCSs (e.g., Figure 4f) is strikingly similar to that of the warm feature identified from interannual correlation (Figure 3a), and to some extent, to the long-term warming trend (Figure 2). We infer that the passage of mobile synoptic waves from the

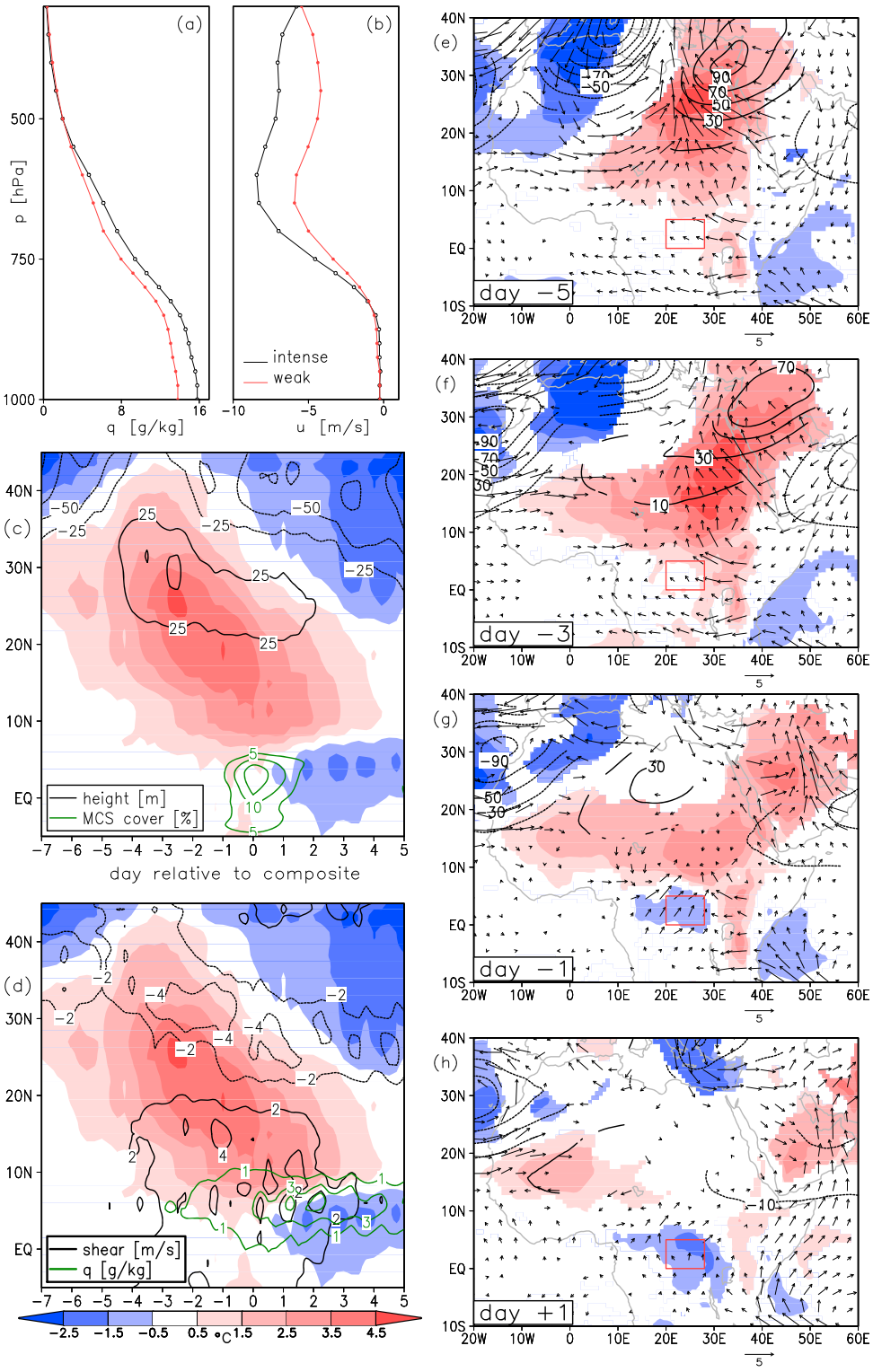

Figure 4. ERA-Interim data composited on intense and weak MCS days in the NE Congo (20–28°E, 0–5°N; red rectangle in (e)–(h)). Vertical profiles at midday on the day of intense (black) and weak (red) events showing (a) specific humidity (g/kg) and (b) zonal wind (m/s). (c) and (d) depict zonal mean (20–28°E) differences between intense and weak composites as a function of latitude and day relative to the MCS event: temperature at 850 hPa (shading; °C); geopotential height at 300 hPa (black contours in (c); m); fractional cover of intense MCS (green contours in (c); %); zonal wind shear between 925 and 600 hPa (black contours in (d); m/s]; specific humidity at 925 hPa (green contours in (d); g/kg). Panels (e) to (h) show differences in wind (vectors) and temperature (shading; both at 850 hPa), and 300 hPa geopotential height (contours) between intense and weak MCS at midday on days −5 (e), −3 (f), −1 (g), and +1 (h) relative to the MCS event. Differences are only plotted where significant at the 95% level according to a two-sample *t* test. MCS = mesoscale convective system.

extratropics triggers strong multiday warming episodes over North-Eastern Africa, exciting the climatological patterns seen in Figure 3a. This provides a mechanistic explanation for the interannual correlations between the upper-level wave pattern, low-level warming in the Eastern Sahel, and intense MCSs in the Congo (Figure 3); years with strong propagating wave activity in North Africa trigger quasi-stationary warming events in the Eastern Sahel, which in turn provide favorable conditions for deeper equatorial MCSs to develop.

Wintertime tropical-extratropical interactions and associated processes related to rainfall anomalies have been studied over West Africa (Cornforth et al., 2017) and the Ethiopian Highlands (Bekele-Biratu et al., 2018; Diro et al., 2011), but to the best of the authors' knowledge, an extratropical link to equatorial MCSs has not previously been found. In West Africa, a northward shift of the wintertime heat low in response to subtropical wave patterns has been noted by Knippertz and Fink (2008), triggering a flux of moist air inland, and dry season rains. However, none of these studies considered the role of wintertime Sahelian warming in enhancing wind shear.

4. Summary and Discussion

Motivated by a previous Sahelian study of MCS intensification, we have examined the relationships between meridional temperature gradient, wind shear, and MCS intensity through the annual cycle in West and central Africa. This analysis highlighted a dramatic rise in intense MCS frequency in February in the N. Congo, accompanied by strong surface warming to the north during that month. Rather than a gradual trend over the 35-year record, both variables exhibited marked increases around 1999; intense MCS frequency increased from one every 3.7 days to one every 2 days, while surface temperatures rose by 2.2 °C in the E. Sahel. As in the Sahelian study, Congo MCS intensification is well correlated with baroclinicity trends, associated with strong warming to the north of the rain belt. Warming in the Eastern Sahel enhances the AEJ over the Northern Congo, providing a more strongly sheared environment favorable for intense MCSs. Event-based analysis strongly supports the link between baroclinicity and MCS intensity; in the days ahead of strong MCSs, temperatures in NE Africa are more than 4 °C warmer than ahead of weak MCSs. The temperature gradient enhances shear and moisture convergence in the N. Congo, both of which likely contribute to more intense organized convection.

A striking aspect of this analysis, and one that certainly merits further investigation, is the seasonality of observed warming, which in turn we assume to be driving MCS intensification. The trend in February warming in the Eastern Sahel is linked to an upper-level geopotential height pattern covering western Eurasia, North-Eastern Africa, and the Middle East. This pattern is reminiscent of the Eastern Atlantic/Western Russia that affects European hydroclimate in later winter/early spring (Ionita, 2014). The zone of maximum warming coincides with a very dry atmosphere yet is in close proximity to much moister conditions (Figure 3c). As in the Sahara during the summer monsoon (Vizy & Cook, 2017), the radiative balance in the Eastern Sahel during February is very sensitive to moisture convergence, and radiative feedbacks may enhance dynamically triggered warming. In subsequent months, the observed warming trend in North Africa becomes more zonally uniform, and we speculate that increasing baroclinicity over West Africa may be contributing to long-term MCS intensification within the Guinea Coast region at latitudes where the AEJ provides strong shear, as suggested by Figure 1. The change in MCS properties during February corresponds to an earlier onset in the intense MCS season over Equatorial and North Africa and is correlated with increased February rainfall. The magnitude of the trends in frequency and temperature for February approach the values found by T17 in the Sahel during the monsoon months of June to September. However, there are important differences between the two studies, notably in the timing of the signal, and its relationship with midlatitudes. Considering timing, a consistent long-term trend in the Sahel dominates over interannual variability, giving rise to strong correlations with global temperature, suggestive of greenhouse gas effects. By contrast in the Congo, there is a notable jump in MCS intensity in 1999, suggesting a dominant role for decadal-scale coupled ocean-atmosphere variability. The nature of that variability, and the extent to which it is a response to anthropogenic forcing, is an important question that remains to be tackled. Second, we highlight a key role for the extratropics in triggering warming in North-Eastern Africa, via an upper-level wave train. At low levels, the warm anomalies propagate southward, extending the heat low into the Eastern Sahel and exciting a quasi-stationary pattern which projects onto the climatological

signal. The enhanced heat low generates additional shear and drives moisture advection into the Congo Basin from the south. The driver of the long-term February warming trend in the Eastern Sahel and resulting MCS intensification appears to be upper-level circulation changes over North-Eastern Africa. Their underlying mechanism remain unclear, as does any potential link to greenhouse warming. Considering future projections across North Africa however, anthropogenic emissions of greenhouse gases are projected to drive enhanced warming in arid and semiarid regions (Zhou, 2016). This is expected to enhance the AEJ and may make shear-sensitive MCSs more efficient at generating intense rain (Alfaro, 2017). As in T17, future trends in extreme rainfall from African MCSs may therefore be controlled by the interplay between within-storm processes and the larger-scale dynamics, as much as by trends in atmospheric moisture. This presents problems for large-scale climate models, which are unable to represent storm dynamics accurately.

Acknowledgments

The research leading to these results received funding from the UK's Natural Environment Research Council (NERC)/ Department for International Development (DFID) Future Climate For Africa programme, under the AMMA-2050 project (grant numbers NE/M020428/1, NE/M019950/1, and NE/M020126/1), and the NERC-funded VERA project (NE/M004295/1). Additional support is acknowledged by Doug Parker for a Royal Society Wolfson Research Merit Award (Doug Parker) and by Andreas Fink within the subproject "Prediction of wet and dry periods of the West African monsoon" of the Transregional Collaborative Research Center SFB/TRR 165 "Waves to Weather" funded by the German Research Foundation (DFG). We thank the providers of key data sets used here, notably Eumetsat, ECMWF, CRU, and NASA. The data used in this study can be freely downloaded from the following locations: www.ncdc.noaa.gov/gridsat (GridSat), crudata.uea.ac.uk/cru/data/hrg (CRU temperature), ghrc.nsstc.nasa.gov/home (MSU temperature), www.ecmwf.int/en/research/climate-reanalysis/era-interim (atmospheric reanalysis data), and disc.gsfc.nasa.gov/datasets/TRMM_3B43_V7/summary (TRMM 3B43 rainfall). We are very grateful for the helpful comments made by the reviewers.

References

Albrecht, R. I., Goodman, S. J., Buechler, D. E., Blakeslee, R. J., & Christian, H. J. (2016). Where are the lightning hotspots on Earth? *Bulletin of the American Meteorological Society*, *97*(11), 2051–2068. https://doi.org/10.1175/BAMS-D-14-00193.1

Alfaro, D. A. (2017). Low-tropospheric shear in the structure of squall lines: Impacts on latent heating under layer-lifting ascent. *Journal of the Atmospheric Sciences*, *74*(1), 229–248. https://doi.org/10.1175/JAS-D-16-0168.1

Bekele-Biratu, E., Thiaw, W. M., & Korecha, D. (2018). Sub-seasonal variability of the Belg rains in Ethiopia. *International Journal of Climatology*, *38*(7), 2940–2953. https://doi.org/10.1002/joc.5474

Christy, J. R., Spencer, R. W., & Braswell, W. D. (2000). MSU tropospheric temperatures: Dataset construction and radiosonde comparisons. *Journal of Atmospheric and Oceanic Technology*, *17*(9), 1153–1170. https://doi.org/10.1175/1520-0426(2000)017<1153:MTTDCA>2.0.CO;2

Cook, K. H., & Vizy, E. K. (2015). Detection and analysis of an amplified warming of the Sahara Desert. *Journal of Climate*, *28*(16), 6560–6580. https://doi.org/10.1175/JCLI-D-14-00230.1

Cornforth, R., Mumba, Z., Parker, D. J., Berry, G., Chapelon, N., Diakaria, K., et al. (2017). Synoptic systems. In D. J. Parker, & M. Diop-Kane (Eds.), *Meteorology of tropical West Africa: The forecasters' handbook*, edited by, (pp. 40–89). Chichester, U.K: John Wiley and Sons, Ltd.

Dee, D. P., Uppala, S. M., Simmons, A. J., Berrisford, P., Poli, P., Kobayashi, S., et al. (2011). The ERA-interim reanalysis: Configuration and performance of the data assimilation system. *Quarterly Journal of the Royal Meteorological Society*, *137*(656), 553–597. https://doi.org/10.1002/qj.828

Diro, G. T., Grimes, D. I. F., & Black, E. (2011). Teleconnections between Ethiopian summer rainfall and sea surface temperature: Part I—Observation and modelling. *Climate Dynamics*, *37*(1), 103–119.

Evan, A. T., Flamant, C., Lavaysse, C., Kocha, C., & Saci, A. (2014). Water vapor–forced greenhouse warming over the Sahara Desert and the recent recovery from the Sahelian drought. *Journal of Climate*, *28*(1), 108–123.

Futyan, J. M., & Genio, A. D. D. (2007). Deep convective system evolution over Africa and the tropical Atlantic. *Journal of Climate*, *20*(20), 5041–5060. https://doi.org/10.1175/JCLI4297.1

Harris, I., Jones, P. D., Osborn, T. J., & Lister, D. H. (2014). Updated high-resolution grids of monthly climatic observations—The CRU TS3.10 dataset. *International Journal of Climatology*, *34*(3), 623–642. https://doi.org/10.1002/joc.3711

Houze, R. A. (2004). Mesoscale convective systems. *Reviews of Geophysics*, *42*, RG4003. https://doi.org/10.1029/2004RG000150

Huang, B., Kennedy, J., Xue, Y., & Zhang, H. M. (2018). Sea surface temperatures. In *State of the climate in 2017*, edited, (pp. S69–S70). *Bulletin of the American Meteorological Society, 99*. https://doi.org/10.1175/2018BAMSStateoftheClimate.1

Huffman, G. J., Bolvin, D. T., Nelkin, E. J., Wolff, D. B., Adler, R. F., Gu, G., et al. (2007). The TRMM multisatellite precipitation analysis (TMPA): Quasi-global, multiyear, combined-sensor precipitation estimates at fine scales. *Journal of Hydrometeorology*, *8*(1), 38–55. https://doi.org/10.1175/JHM560.1

Ionita, M. (2014). The impact of the East Atlantic/Western Russia pattern on the hydroclimatology of Europe from mid-winter to late spring. *Climate*, *2*(4), 296–309. https://doi.org/10.3390/cli2040296

Jackson, B., Nicholson, S. E., & Klotter, D. (2009). Mesoscale convective systems over western equatorial Africa and their relationship to large-scale circulation. *Monthly Weather Review*, *137*(4), 1272–1294. https://doi.org/10.1175/2008MWR2525.1

Jones, P. D., Lister, D. H., Osborn, T. J., Harpham, C., Salmon, M., & Morice, C. P. (2012). Hemispheric and large-scale land-surface air temperature variations: An extensive revision and an update to 2010. *Journal of Geophysical Research*, *117*, D05127. https://doi.org/10.1029/2011JD017139

Kai, L., Geert, L., & Pier, S. A. (2017). The spatial extent of rainfall events and its relation to precipitation scaling. *Geophysical Research Letters*, *44*, 8629–8636.

Klein, C., Belušić, D., & Taylor, C. M. (2018). Wavelet scale analysis of mesoscale convective systems for detecting deep convection from infrared imagery. *Journal of Geophysical Research: Atmospheres*, *123*, 3035–3050. https://doi.org/10.1002/2017JD027432

Knapp, K. R. (2008). Calibration assessment of ISCCP geostationary infrared observations using HIRS. *Journal of Atmospheric and Oceanic Technology*, *25*(2), 183–195. https://doi.org/10.1175/2007JTECHA910.1

Knapp, K. R., Ansari, S., Bain, C. L., Bourassa, M. A., Dickinson, M. J., Funk, C., et al. (2011). Globally gridded satellite observations for climate studies. *Bulletin of the American Meteorological Society*, *92*(7), 893–907. https://doi.org/10.1175/2011BAMS3039.1

Knippertz, P., & Fink, A. H. (2008). Dry-season precipitation in tropical West Africa and its relation to forcing from the extratropics. *Monthly Weather Review*, *136*(9), 3579–3596. https://doi.org/10.1175/2008MWR2295.1

Laing, A. G., Carbone, R. E., & Levizzani, V. (2011). Cycles and propagation of deep convection over equatorial Africa. *Monthly Weather Review*, *139*(9), 2832–2853. https://doi.org/10.1175/2011MWR3500.1

Lavaysse, C., Flamant, C., Janicot, S., Parker, D. J., Lafore, J. P., Sultan, B., & Pelon, J. (2009). Seasonal evolution of the West African heat low: A climatological perspective. *Climate Dynamics*, *33*(2), 313–330.

Lenderink, G., & van Meijgaard, E. (2008). Increase in hourly precipitation extremes beyond expectations from temperature changes. *Nature Geoscience*, *1*(8), 511–514. https://doi.org/10.1038/ngeo262

Maidment, R. I., David, G., P, A. R., Elena, T., Marc, S., Tim, H., Rob, R., et al. (2014). The 30 year TAMSAT African Rainfall Climatology and Time series (TARCAT) data set. *Journal of Geophysical Research: Atmospheres*, *119*, 10,619–610,644. https://doi.org/10.1002/2014JD021927

Maranan, M., Fink, A. H., & Knippertz, P. (2018). Rainfall types over southern West Africa: Objective identification, climatology and synoptic environment. *Quarterly Journal of the Royal Meteorological Society*, *144*(714), 1628–1648. https://doi.org/10.1002/qj.3345

Mathon, V., Laurent, H., & Lebel, T. (2002). Mesoscale convective system rainfall in the Sahel. *Journal of Applied Meteorology*, *41*(11), 1081–1092. https://doi.org/10.1175/1520-0450(2002)041<1081:MCSRIT>2.0.CO;2

Min, S.-K., Zhang, X., Zwiers, F. W., & Hegerl, G. C. (2011). Human contribution to more-intense precipitation extremes. *Nature*, *470*(7334), 378–381. https://doi.org/10.1038/nature09763

Muller, C. (2013). Impact of convective organization on the response of tropical precipitation extremes to warming. *Journal of Climate*, *26*(14), 5028–5043. https://doi.org/10.1175/JCLI-D-12-00655.1

Nesbitt, S. W., Cifelli, R., & Rutledge, S. A. (2006). Storm morphology and rainfall characteristics of TRMM precipitation features. *Monthly Weather Review*, *134*(10), 2702–2721. https://doi.org/10.1175/MWR3200.1

O'Gorman, P. A. (2015). Precipitation extremes under climate change. *Current Climate Change Reports*, *1*(2), 49–59. https://doi.org/10.1007/s40641-015-0009-3

Prein, A. F., Liu, C., Ikeda, K., Trier, S. B., Rasmussen, R. M., Holland, G. J., & Clark, M. P. (2017). Increased rainfall volume from future convective storms in the US. *Nature Climate Change*, *7*(12), 880–884. https://doi.org/10.1038/s41558-017-0007-7

Proud, S. R. (2015). Analysis of overshooting top detections by Meteosat second generation: A 5-year dataset. *Quarterly Journal of the Royal Meteorological Society*, *141*(688), 909–915. https://doi.org/10.1002/qj.2410

Raghavendra, A., Zhou, L., Jiang, Y., & Hua, W. (2018). Increasing extent and intensity of thunderstorms observed over the Congo Basin from 1982 to 2016. *Atmospheric Research*, *213*, 17–26. https://doi.org/10.1016/j.atmosres.2018.05.028

Rayner, N. A., Parker, D. E., Horton, E. B., Folland, C. K., Alexander, L. V., Rowell, D. P., et al. (2003). Global analyses of sea surface temperature, sea ice, and night marine air temperature since the late nineteenth century. *Journal of Geophysical Research*, *108*(D14), 4407. https://doi.org/10.1029/2002JD002670

Rotunno, R., Klemp, J. B., & Weisman, M. L. (1988). A theory for strong, long-lived squall lines. *Journal of the Atmospheric Sciences*, *45*(3), 463–485. https://doi.org/10.1175/1520-0469(1988)045<0463:ATFSLL>2.0.CO;2

Singleton, A., & Toumi, R. (2013). Super-Clausius–Clapeyron scaling of rainfall in a model squall line. *Quarterly Journal of the Royal Meteorological Society*, *139*(671), 334–339. https://doi.org/10.1002/qj.1919

Taylor, C. M., Belušić, D., Guichard, F., Parker, D. J., Vischel, T., Bock, O., et al. (2017). Frequency of extreme Sahelian storms tripled since 1982 in satellite observations. *Nature*, *544*(7651), 475–478. https://doi.org/10.1038/nature22069

Thorpe, A. J., Miller, M. J., & Moncrieff, M. W. (1982). 2-dimensional convection in non-constant shear—A model of mid-latitude squall lines. *Quarterly Journal of the Royal Meteorological Society*, *108*(458), 739–762. https://doi.org/10.1002/qj.49710845802

Vizy, E. K., & Cook, K. H. (2017). Seasonality of the observed amplified Sahara warming trend and implications for Sahel rainfall. *Journal of Climate*, *30*(9), 3073–3094. https://doi.org/10.1175/JCLI-D-16-0687.1

Westra, S., Alexander, L. V., & Zwiers, F. W. (2013). Global increasing trends in annual maximum daily precipitation. *Journal of Climate*, *26*(11), 3904–3918. https://doi.org/10.1175/JCLI-D-12-00502.1

Westra, S., Fowler, H. J., Evans, J. P., Alexander, L. V., Berg, P., Johnson, F., et al. (2014). Future changes to the intensity and frequency of short-duration extreme rainfall. *Reviews of Geophysics*, *52*, 522–555. https://doi.org/10.1002/2014RG000464

Zhou, L. (2016). Desert amplification in a warming climate. *Scientific Reports*, *6*(1), 31065. https://doi.org/10.1038/srep31065

Zhou, L., Tian, Y., Myneni, R. B., Ciais, P., Saatchi, S., Liu, Y. Y., et al. (2014). Widespread decline of Congo rainforest greenness in the past decade. *Nature*, *509*(7498), 86–90. https://doi.org/10.1038/nature13265

Zipser, E. J., Liu, C., Cecil, D. J., Nesbitt, S. W., & Yorty, D. P. (2006). Where are the most intense thunderstorms on Earth? *Bulletin of the American Meteorological Society*, *87*(8), 1057–1072. https://doi.org/10.1175/BAMS-87-8-1057